Translation of quantum states by four-wave mixing in fibers

C. J. McKinstrie,[1] J. D. Harvey,[2] S. Radic[3] and M. G. Raymer[4]

[1]*Bell Laboratories, Lucent Technologies, Holmdel, New Jersey 07733*
[2]*Department of Physics, University of Auckland, Private Bag 92019, Auckland, New Zealand*
[3]*Department of Electrical and Computer Engineering, University of California at San Diego, La Jolla, California 92093*
[4]*Oregon Center for Optics and Department of Physics, University of Oregon, Eugene, Oregon 97403*

mckinstrie@lucent.com

Abstract: Optical frequency conversion by four-wave mixing (Bragg scattering) in a fiber is considered. If the frequencies and polarizations of the waves are chosen judiciously, Bragg scattering enables the translation of individual and entangled states, without the noise pollution associated with parametric amplification (modulation instability or phase conjugation), and with reduced noise pollution associated with stimulated Raman scattering.

OCIS codes: (060.4370) nonlinear optics, fibers; (190.2620) frequency conversion; (270.2500) fluctuations, relaxation and noise.

References and links

1. J. Hansryd, P. A. Andrekson, M. Westlund, J. Li and P. O. Hedekvist, "Fiber-based optical parametric amplifiers and their applications," IEEE J. Sel. Top. Quantum Electron. **8**, 506–520 (2002).
2. S. Radic and C. J. McKinstrie, "Two-pump fiber parametric amplifiers," Opt. Fiber Technol. **9**, 7–23 (2003).
3. W. H. Louisell, *Radiation and Noise in Quantum Electronics* (McGraw-Hill, 1964).
4. R. Loudon, *The Quantum Theory of Light, 3rd Ed.* (Oxford University Press, 2000).
5. C. J. McKinstrie, S. Radic and M. G. Raymer, "Quantum noise properties of parametric amplifiers driven by two pump waves," Opt. Express **12**, 5037–5066 (2004).
6. C. J. McKinstrie, M. Yu, M. G. Raymer and S. Radic, "Quantum noise properties of parametric processes," Opt. Express **13**, 4986–5012 (2005).
7. M. G. Raymer, "Quantum state entanglement and readout of collective atomic-ensemble modes and optical wave packets by stimulated Raman scattering," J. Mod. Opt. **51**, 1739–1759 (2004).
8. H. Kogelnik, R. M. Jopson and L. E. Nelson, "Polarization-mode dispersion," in *Optical Fiber Telecommunications IVB*, edited by I. Kaminow and T. Li (Academic Press, 2002), pp. 725–861.
9. C. J. McKinstrie, S. Radic and A. R. Chraplyvy, "Parametric amplifiers driven by two pump waves," IEEE J. Sel. Top. Quantum Electron. **8**, 538–547 and 956 (2002).
10. C. J. McKinstrie, S. Radic and C. Xie, "Parametric instabilities driven by orthogonal pump waves in birefringent fibers," Opt. Express **11**, 2619–2633 (2003).
11. C. J. McKinstrie, H. Kogelnik, R. M. Jopson, S. Radic and A. V. Kanaev, "Four-wave mixing in fibers with random birefringence," Opt. Express **12**, 2033–2055 (2004).
12. M. Yu, C. J. McKinstrie and G. P. Agrawal, "Modulational instabilities in dispersion-flattened fibers," Phys. Rev. E **52**, 1072–1080 (1995).
13. J. D. Harvey, R. Leonhardt, S. Coen, G. K. L. Wong, J. C. Knight, W. J. Wadsworth and P. S. J. Russell, "Scalar modulation instability in the normal dispersion regime by use of a photonic crystal fiber," Opt. Lett. **28**, 2225–2227 (2003).
14. A. Y. H. Chen, G. K. L. Wong, S. G. Murdoch, R. Leonhardt, J. D. Harvey, J. C. Knight, W. J. Wadsworth and P. S. J. Russell, "Widely tunable optical parametric generation in a photonic crystal fiber," Opt. Lett. **30**, 762–764 (2005).

#8674 - $15.00 USD Received 6 September 2005; revised 26 October 2005; accepted 30 October 2005

15. T. Tanemura, J. Suzuki, K. Katoh and K. Kikuchi, "Polarization-insensitive all-optical wavelength conversion using cross-phase modulation in twisted fiber and optical filtering," IEEE Photon. Technol. Lett. **17**, 1052–1054 (2005).
16. R. H. Stolen and E. P. Ippen, "Raman gain in glass optical waveguides," Appl. Phys. Lett. **22**, 276–278 (1973).
17. R. H. Stolen, "Polarization effects in fiber Raman and Brillouin lasers," IEEE J. Quantum Electron. **15**, 1157–1160 (1979).
18. M. G. Raymer and I. A. Walmsley, "Quantum coherence properties of stimulated Raman scattering," in *Progress in Optics, Vol. 28*, edited by E. Wolf (North-Holland, 1990), pp. 181–270.
19. P. L. Voss and P. Kumar, "Raman-noise-induced noise-figure limit for $\chi^{(3)}$ parametric amplifiers," Opt. Lett. **29**, 445–447 (2004).
20. R. Tang, P. L. Voss, J. Lasri, P. Devgan and P. Kumar, "Noise-figure limit of fiber-optical parametric amplifiers and wavelength convertors: experimental investigation," Opt. Lett. **29**, 2372–2374 (2004).
21. X. Li, P. L. Voss, J. Chen, K. F. Lee and P. Kumar, "Measurement of co- and cross-polarized Raman spectra in silica fiber for small detunings," Opt. Express **13**, 2236-2244 (2005).
22. P. D. Maker and R. W. Terhune, "Study of optical effects due to an induced polarization third order in the electric field strength," Phys. Rev. **137**, A801–A818 (1965).
23. P. K. A. Wai, C. R. Menyuk and H. H. Chen, "Stability of solitons in randomly varying birefringent fibers," Opt. Lett. **16**, 1231–1233 (1991).
24. S. G. Evangelides, L. F. Mollenauer, J. P. Gordon and N. S. Bergano, "Polarization muliplexing with solitons," J. Lightwave Technol. **10**, 28–35 (1992).
25. C. R. Menyuk, "Nonlinear pulse propagation in birefringent optical fibers," IEEE J. Quantum Electron. **23**, 174–176 (1987).
26. A. J. Barlow, J. J. Ramskov-Hansen and D. N. Payne, "Birefringence and polarization-mode dispersion in spun single-mode fibers," Appl. Opt. **20**, 2962–2968 (1981).

1. Introduction

In many optical systems, the required photon frequencies differ from the frequencies at which the transmitters emit photons or the receivers detect them efficiently. For this reason, optical frequency conversion (FC) is important. Parametric amplification (PA) in a fiber is based on four-wave mixing (FWM). Not only does FWM produce amplified signals, it also produces idlers that are frequency-shifted and phase-conjugated images of the signals. Consequently, PAs have many uses in classical communication systems [1, 2]. However, with amplification comes noise [3, 4]. Although this noise might not impair the performance of classical (many-photon) systems, it does change the characteristics of quantal (few-photon) systems. Consequently, PAs must be used with caution in few-photon systems.

PA driven by two pump waves (1 and 2) involves four product waves (sidebands) that are coupled by three distinct FWM processes, as illustrated in Fig. 1. Suppose that the signal fre-

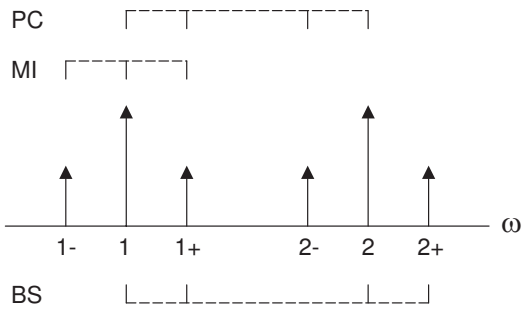

Fig. 1. Illustration of the constituent two-mode processes in a four-mode parametric interaction driven by two pump waves.

quency $\omega_{1+} = \omega_1 + \omega$, where ω is the modulation frequency, and let γ denote a photon. Then

#8674 - $15.00 USD Received 6 September 2005; revised 26 October 2005; accepted 30 October 2005

the modulation interaction (MI) in which $2\gamma_1 \rightarrow \gamma_{1-} + \gamma_{1+}$ produces an idler with frequency $\omega_{1-} = \omega_1 - \omega$, the phase-conjugation (PC) process in which $\gamma_1 + \gamma_2 \rightarrow \gamma_{1+} + \gamma_{2-}$ produces an idler with frequency $\omega_{2-} = \omega_2 - \omega$ and the Bragg scattering (BS), or FC, process in which $\gamma_{1+} + \gamma_2 \rightarrow \gamma_1 + \gamma_{2+}$ produces an idler with frequency $\omega_{2+} = \omega_2 + \omega$. In MI and PC, pump photons are destroyed in pairs, whereas sideband (signal and idler) photons are produced in pairs. This behavior enables signal amplification and idler generation. However, it also enables the vacuum fluctuations associated with the signal and idler to be amplified: (excess) noise is produced [5, 6]. In BS, for each idler photon that is created, a signal photon is destroyed: Power is transferred from the signal to the idler. Because the total sideband power is constant, the vacuum fluctuations are not amplified: no (excess) noise is produced [5, 6]. This distinctive feature of BS suggests that it might be useful for FC in few-photon systems.

2. State translation by Bragg scattering

In studies of FWM it is customary to use a classical model for the strong (constant-amplitude) pumps (1 and 2) and a quantal model for the weak (variable-amplitude) sidebands (1+ and 2+). In this paper the 1+ sideband is the signal (s) and the 2+ sideband is the idler (i). The analysis of the complementary case, in which the 2+ sideband is the signal and the 1+ sideband is the idler, is similar. BS in a $\chi^{(3)}$ medium, such as a fiber, is governed by the Hamiltonian

$$H = \delta(a_s^\dagger a_s - a_i^\dagger a_i) + \kappa a_s^\dagger a_i + \kappa^* a_s a_i^\dagger, \tag{1}$$

together with the (spatial) Heisenberg equations-of-motion

$$d_z a_j = i[a_j, H], \tag{2}$$

where $d_z = d/dz$ and $j = s$ or i [3, 4, 5, 6]. In Eqs. (1) and (2), each a is a destruction operator and each hermitian conjugate $a^\dagger$ is a creation operator. These operators satisfy the boson commutation relations $[a_j, a_k] = 0$ and $[a_j, a_k^\dagger] = \delta_{jk}$, where δ_{jk} is the Kronecker delta and $k = s$ or i. The parameters δ and κ quantify the effects of wavenumber mismatch and pump-induced coupling, respectively.

By combining Eqs. (1) and (2), one obtains the operator equations

$$d_z a_s = i\delta a_s + i\kappa a_i, \tag{3}$$
$$d_z a_i = i\kappa^* a_s - i\delta a_i. \tag{4}$$

The solutions of Eqs. (3) and (4) can be written in the input-output form

$$a_s(z) = \bar{\mu}(z) a_s(0) + \bar{\nu}(z) a_i(0), \tag{5}$$
$$a_i(z) = -\bar{\nu}^*(z) a_s(0) + \bar{\mu}^*(z) a_i(0), \tag{6}$$

where the transfer functions

$$\bar{\mu}(z) = \cos(kz) + i\delta \sin(kz)/k, \tag{7}$$
$$\bar{\nu}(z) = i\kappa \sin(kz)/k \tag{8}$$

and the BS wavenumber $k = (|\kappa|^2 + \delta^2)^{1/2}$. The transfer functions satisfy the auxiliary equation $|\bar{\mu}|^2 + |\bar{\nu}|^2 = 1$, which ensures that the BS transformation is unitary and conserves photons. Equations (5) and (6) have the same form as the equations for parametric frequency upconversion in a $\chi^{(2)}$ medium [3] and anti-Stokes scattering in a Raman medium [7].

Consider the effects of BS on an input that consists of one signal photon and no idler photons. The state vector associated with such an input is denoted by $|1,0\rangle$. In the Heisenberg picture

#8674 - $15.00 USD Received 6 September 2005; revised 26 October 2005; accepted 30 October 2005

the state vector remains constant while the mode operators evolve. It is a matter of convenience whether one expresses the state vector in terms of the input or output modes. By recognizing that $|1,0\rangle_{\rm in} = a_s^\dagger(0)|0,0\rangle_{\rm in}$ and $|0,0\rangle_{\rm in} = |0,0\rangle_{\rm out}$, and using the inverse of Eq. (5) to rewrite the input-mode operator $a_s^\dagger(0)$ in terms of the output-mode operators $a_s^\dagger(z)$ and $a_i^\dagger(z)$, one finds that

$$|1,0\rangle_{\rm in} = \bar{\mu}|1,0\rangle_{\rm out} - \bar{\nu}^*|0,1\rangle_{\rm out}. \tag{9}$$

Hence, if $|\bar{\nu}| = 1$ ($|\bar{\mu}| = 0$), the output state $|0,1\rangle$ is a perfect frequency-shifted (translated) image of the input state $|1,0\rangle$. Because the phase of the state vector has no physical meaning, this statement is true for arbitrary $\phi_{\bar{\nu}} = \arg(\bar{\nu})$.

Similar results apply to other one-mode input states. Consider the input $|s,0\rangle = \sum_n c_n|n,0\rangle$, where s is the label for the signal state (not a photon number). In abbreviated notation, $|s\rangle = \sum_n c_n|n\rangle_s$, where $|n\rangle_s$ is a signal number-state. The first-order (field-amplitude) moment $\langle a_s\rangle = \sum_n c_n^* c_{n+1}(n+1)^{1/2}$ and the second-order (photon-number) moment $\langle a_s^\dagger a_s\rangle = \sum_n |c_n|^2 n$. It follows from Eq. (9) and the identity $|n\rangle = (a^\dagger)^n|0\rangle/(n!)^{1/2}$ that the output $|0,i\rangle = \sum_n c_n e^{in\phi}|0,n\rangle$, where $\phi = \pi - \phi_{\bar{\nu}}$. In abbreviated notation, $|i\rangle = \sum_n c_n e^{in\phi}|n\rangle_i$, where $|n\rangle_i$ is an idler number-state. In the number-state expansions of the input and output states, the idler coefficients differ from the signal coefficients by factors of $e^{in\phi}$. The first-order moment $\langle a_i\rangle = \sum_n c_n^* c_{n+1}(n+1)^{1/2}e^{i\phi}$ and the second-order moment $\langle a_i^\dagger a_i\rangle = \sum_n |c_n|^2 n$. By comparing the signal and idler formulas, one finds that the signal and idler phases differ by ϕ, whereas their magnitudes and numbers are equal. Similar results can be derived for the higher-order moments, such as the amplitude and number variances. It follows from these results that the probability distributions of the signal and idler amplitudes are related by a rigid rotation in the complex plane, whereas the number variances of the signal and idler are equal. For example, if the input is a coherent signal, the output is a coherent idler.

Now suppose that the input consists of two signal photons, denoted by s and s', and no idler photons. These photons could have different frequencies or polarizations, and they could be independent (produced by different lasers) or correlated (produced by prior MI or PC). In any case, the Hamiltonian contains two terms of the form (1). The first term pertains to s and i, whereas the second pertains to s' and i'. The second pair of signal and idler modes also satisfies the commutation relations stated after Eq. (2). Furthermore, $[a', a] = 0$ and $[a', a^\dagger] = 0$, where a is a signal or an idler mode. These relations imply that the composite evolution operator can be written as the product of two individual evolution operators, one for each pair of signal and idler modes: Each pair evolves independently of the other. Let $|1,0;1,0\rangle$ denote the input state. Then, by following the procedure described above, one finds that

$$\begin{aligned} |1,0;1,0\rangle_{\rm in} \;=\; & \bar{\mu}\bar{\mu}'|1,0;1,0\rangle_{\rm out} - \bar{\mu}(\bar{\nu}')^*|1,0;0,1\rangle_{\rm out} \\ & - \bar{\nu}^*\bar{\mu}'|0,1;1,0\rangle_{\rm out} + \bar{\nu}^*(\bar{\nu}')^*|0,1;0,1\rangle_{\rm out}. \end{aligned} \tag{10}$$

Hence, if $|\bar{\nu}| = 1$ and $|\bar{\nu}'| = 1$ simultaneously, the output state $|0,1;0,1\rangle$ is a perfect image of the input state $|1,0;1,0\rangle$.

Similar results apply to other two-mode input states. The input $|s,0;s',0\rangle = \sum_n \sum_{n'} c_{nn'}$ $|n,0;n',0\rangle$, which has the abbreviated form $|s;s'\rangle = \sum_n \sum_{n'} c_{nn'}|n;n'\rangle_s$, becomes the output $|i;i'\rangle$ $= \sum_n \sum_{n'} c_{nn'} e^{i(n\phi+n'\phi')}|n;n'\rangle_i$. For example, if the input consists of two coherent signals (in which case the input state is the product of two one-mode superposition states and two vacuum states), the output consists of two coherent (and phase-shifted) idlers. If the input is the entangled state $|0;0'\rangle_s + |1;1'\rangle_s$, the output is the entangled state $|0;0'\rangle_i + e^{i(\phi+\phi')}|1;1'\rangle_i$.

3. Bragg scattering in a highly-nonlinear fiber

Several different types of fiber exist. Asymmetric single-mode fibers (SMFs) and microstructured fibers (MSFs) are birefringent and polarization-maintaining. Highly-nonlinear fibers

#8674 - $15.00 USD Received 6 September 2005; revised 26 October 2005; accepted 30 October 2005

(HNFs), which are symmetric SMFs with small effective areas, are non-birefringent and non-polarization-maintaining. Although the absolute polarizations of the pumps, signals and idlers vary with distance in a HNF, the relative polarizations remain constant, provided that the HNF is not too long or the frequency differences between the waves are not too large [8]. FWM in both types of fiber has been studied in detail [9, 10, 11]. This paper focuses on BS in HNFs, because these fibers enabled the recent progress in parametric signal processing [1, 2]. For comparison, BS in asymmetric SMFs and MSFs is discussed briefly in the Appendix.

In a HNF the BS mismatch $\delta = (\beta_s + \beta_2 - \beta_i - \beta_1)/2 + \gamma(P_1 - P_2)/2$, where each β is a wavenumber, γ is the (Kerr) nonlinearity coefficient (multiplied by a factor of 8/9) and each $P = |A|^2$ is a pump power [11]. For the configuration shown in Fig. 2(a), the coupling coefficient $\kappa_{\|} = 2\gamma A_1 A_2^*$, whereas for the configurations shown in Figs. 2(b) and 3(a), $\kappa_{\perp} = \gamma A_1 A_2^*$.

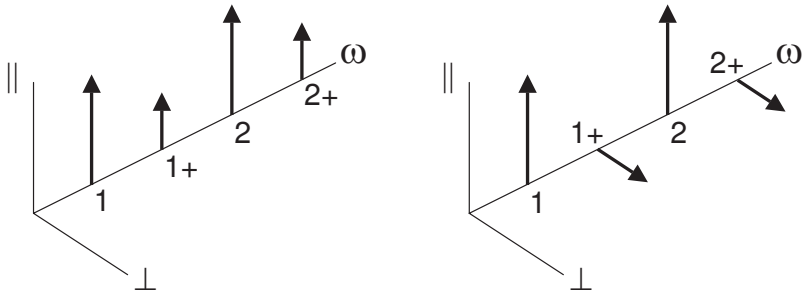

Fig. 2. Eigenpolarizations of BS driven by parallel pumps.

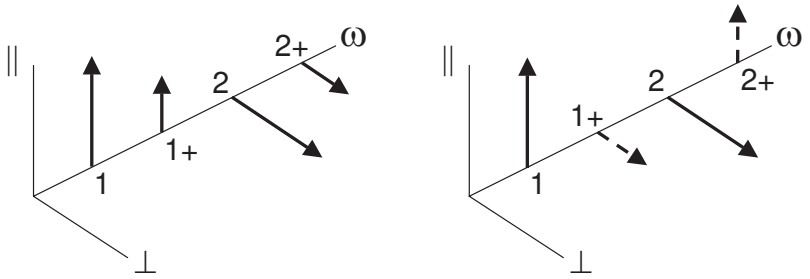

Fig. 3. Eigenpolarizations of BS driven by perpendicular pumps. The dashed lines denote sidebands that propagate independently.

For the configuration shown in Fig. 3(b), $\kappa = 0$. The configurations shown in Fig. 2 produce idlers that are parallel to the signals, whereas the configuration shown in Fig. 3(a) produces an idler that is perpendicular to the signal. In Figs. 2 and 3 the symbol $\|$ refers to any polarization (Jones) vector that is used for reference and the symbol $\perp$ refers to any other vector that is orthogonal (perpendicular) to it. For example, these vectors could represent perpendicular linearly-polarized states, or counter-rotating circularly-polarized states.

4. Translation of individual states

Consider the case in which the signal frequency (ω_s) and the second-pump frequency (ω_2) are fixed. One can vary (tune) the idler frequency (ω_i) by varying the first-pump frequency

#8674 - $15.00 USD Received 6 September 2005; revised 26 October 2005; accepted 30 October 2005

(ω_1). It is convenient to define the auxiliary frequencies $\omega_a = (\omega_s + \omega_2)/2$, $\omega_b = (\omega_2 - \omega_s)/2$ and $\omega_c = (\omega_i - \omega_1)/2$, in terms of which $\omega_1 = \omega_a - \omega_c$, $\omega_s = \omega_a - \omega_b$, $\omega_2 = \omega_a + \omega_b$ and $\omega_i = \omega_a + \omega_c$. All frequencies are measured relative to the zero-dispersion frequency (ZDF) ω_0. By Taylor expanding the mismatch about the average frequency ω_a, one finds that

$$\delta = \beta_2(\omega_b^2 - \omega_c^2)/2 + \beta_4(\omega_b^4 - \omega_c^4)/24, \quad (11)$$

$$= [(\omega_b^2 - \omega_c^2)/2][\beta_2 + \beta_4(\omega_b^2 + \omega_c^2)/12], \quad (12)$$

where β_2 and β_4 are abbreviations for the second- and fourth-order dispersion coefficients $\beta^{(2)}(\omega_a) \approx \beta^{(3)}(\omega_0)\omega_a$ and $\beta^{(4)}(\omega_a) \approx \beta^{(4)}(\omega_0)$, respectively. Equations (11) and (12) apply to typical cases in which $P_2 = P_1 = P$. By varying ω_1, one varies ω_c ($d\omega_c/d\omega_1 = -1$). It follows from Eq. (11) that

$$d\delta/d\omega_1 = \omega_c(\beta_2 + \beta_4\omega_c^2/6), \quad (13)$$

$$d^2\delta/d\omega_1^2 = -(\beta_2 + \beta_4\omega_c^2/2). \quad (14)$$

First, suppose that $\beta_2 = 0$. Then $\delta = 0$ if and only if $\omega_c = \pm\omega_b$. The $+$ sign corresponds to $\omega_1 = \omega_s$ and $\omega_i = \omega_2$, whereas the $-$ sign corresponds to $\omega_1 = \omega_2$ and $\omega_i = \omega_s$. Because $d\delta/d\omega_c \neq 0$, the aforementioned values of ω_c are single roots of the polynomial equation $\delta(\omega_c) = 0$. If the difference frequency is low ($\omega_b \ll |\gamma P/\beta_4|^{1/4}$), Eq. (11) implies that the bandwidth over which the idler frequency can be tuned is of order $|24\gamma P/\beta_4|^{1/4}$. Conversely, if the difference frequency is high, Eq. (13) implies that the tuning bandwidth is of order $|6\gamma P/\beta_4\omega_b^3|$. In this case the tuning bandwidth depends sensitively on β_4, and even more sensitively on ω_b.

Second, suppose that $\beta_2 \neq 0$. Then, just as one can modify the frequency response of MI and PC by choosing β_2 to compensate (partially) the effects of β_4 [12, 13, 14], so also can one modify the frequency response of BS. It follows from Eq. (12) that one can make any value of ω_c a root of the polynomial equation (produce an idler with arbitrary frequency) by setting $\beta_2 + \beta_4(\omega_b^2 + \omega_c^2)/12 = 0$, in which case $d\delta/d\omega_1 = \beta_4\omega_c(\omega_c^2 - \omega_b^2)/12$. If $\omega_c \gg \omega_b$, the tuning bandwidth is of order $|12\gamma P/\beta_4\omega_c^3|$, and depends sensitively on β_4 and ω_c. One can also make ω_b a double root by setting $\beta_2 + \beta_4\omega_b^2/6 = 0$, in which case $d^2\delta/d\omega_1^2 = -\beta_4\omega_b^2/3$ and the tuning bandwidth is of order $|6\gamma P/\beta_4\omega_b^2|^{1/2}$. The tuning bandwidth depends less sensitively on β_4 and ω_b (ω_c) in the double-root case than in the single-root case.

In Fig. 4 the signal and idler transmittances are plotted as functions of the first-pump frequency, for cases in which $\beta_3 = 0.1$ ps^3/Km, $\beta_4 = 10^{-4}$ ps^4/Km, $\gamma = 10$/Km-W, $P = 0.3$ W and $l = 0.26$ Km (parallel pumps) or 0.52 Km (perpendicular pumps). In Fig. 4(a) the signal

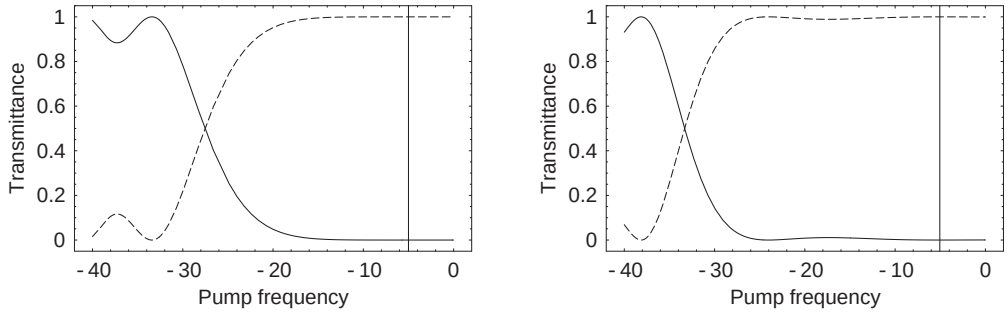

Fig. 4. Signal transmittance (solid curve) and idler transmittance (dashed curve) plotted as functions of the pump frequency ω_1. The vertical line denotes the signal frequency ω_s. (a) $\omega_s = -5.0$ and $\omega_2 = 5.0$ Tr/s. (b) $\omega_s = -5.05$ and $\omega_2 = 4.95$.

and second-pump frequencies are symmetric relative to the ZDF, so $\omega_1 = -5.0$ Tr/s is a single

#8674 - $15.00 USD Received 6 September 2005; revised 26 October 2005; accepted 30 October 2005

root of the polynomial equation $\delta(\omega_1) = 0$. As the first-pump frequency varies from -18 to 0, the idler frequency varies from 18 to 0: The maximal frequency shift is 23. In Fig. 4(*b*) the signal and second-pump frequencies are asymmetric, and the second root $\omega_1 \approx -24$. As the first-pump frequency varies from -28 to 0, the idler frequency varies from about 28 to 0: The maximal frequency shift is about 33.

In Fig. 5 the signal and idler transmittances are plotted as functions of the first-pump frequency, for the same fiber and power parameters as Fig. 4. In Fig. 5(*a*) the signal and second-

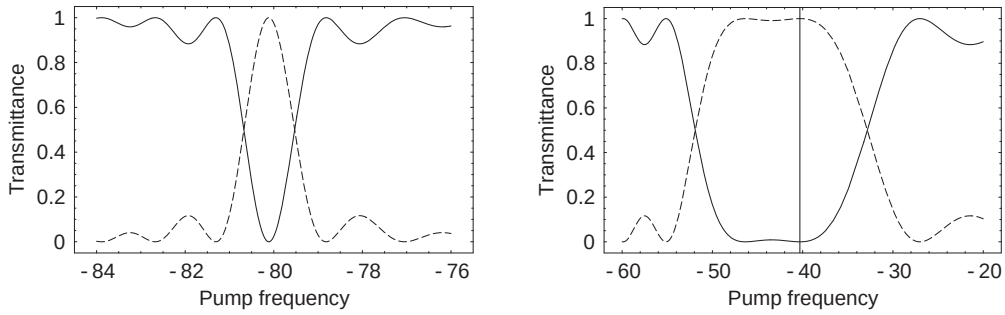

Fig. 5. Signal transmittance (solid curve) and idler transmittance (dashed curve) plotted as functions of the pump frequency ω_1. The vertical line denotes the signal frequency ω_s. (*a*) $\omega_s = -5.53$ and $\omega_2 = 4.47$ Tr/s. (*b*) $\omega_s = -40.31$ and $\omega_2 = 39.69$.

pump frequencies were chosen to produce a narrow tuning band (single root) for $\omega_1 \approx -80$ Tr/s. For this value of the first-pump frequency, the idler frequency is about 80, so the frequency shift is about 85. In Fig. 5(*b*) the signal and second-pump frequencies were chosen to produce a broader tuning band (adjacent roots). As the first-pump frequency varies from -48 to -38, the idler frequency varies from about 48 to 38: The frequency shift varies from about 88 to 78. In Fig. 5(*b*) the pump frequency is comparable to the signal frequency. This condition allows the MI and PC idlers ($1-$ and $2-$, respectively) to be driven near-resonantly. Four-sideband interactions driven by parallel and perpendicular pumps were studied in [9] and [10], respectively. In the first case all four sidebands are parallel to the pumps, whereas in the second case the $1-$ and $1+$ sidebands are parallel to pump 1, and the $2-$ and $2+$ sidebands are parallel to pump 2: The configurations shown in Figs. 2(*a*) and 3(*a*) are susceptible to four-sideband effects (such as parametric amplification and noise production), whereas the configuration shown in Fig. 2(*b*) is not.

5. Translation of frequency-entangled states

Section 4 contained a discussion of how the idler frequency can be varied when the signal frequency is fixed. This information is useful for applications in which one needs to translate a state with one frequency component. In this section the translation of a state with two frequency components (ω_s and ω_s') is discussed. These component states could be independent, correlated or entangled. The distortionless translation of such a state requires that $|\overline{v}|^2 = 1$ and $|\overline{v}'|^2 = 1$ ($\delta = 0$ and $\delta' = 0$) simultaneously. This requirement prompts a discussion of how the idler transmittance (mismatch) depends on the signal frequency, for fixed pump frequencies.

The mismatch and the auxiliary frequencies were defined in Section 4. (For fixed pump frequencies, $d\omega_a/d\omega_s = 1/2$, $d\omega_b/d\omega_s = -1/2$ and $d\omega_c/d\omega_s = 1/2$.) It follows from Eq. (11), in which $\beta_2 = \beta_3\omega_a$, that

$$d\delta/d\omega_s = \beta_3(\omega_b^2 - \omega_c^2)/4 - \beta_3\omega_a(\omega_b + \omega_c)/2 - \beta_4(\omega_b^3 + \omega_c^3)/12, \quad (15)$$

$$d^2\delta/d\omega_s^2 = -\beta_3(\omega_b + \omega_c)/2 + \beta_4(\omega_b^2 - \omega_c^2)/8. \quad (16)$$

#8674 - $15.00 USD Received 6 September 2005; revised 26 October 2005; accepted 30 October 2005

Equation (12) implies that $\delta = 0$ if $\omega_c = \pm\omega_b$. The + sign corresponds to $\omega_s = \omega_1$, whereas the − sign corresponds to $\omega_1 = \omega_2$. Because the frequency shift $\omega_i - \omega_s = \omega_2 - \omega_1$, the latter case is of no interest. Equation (12) also implies that $\delta = 0$ if $\beta_3\omega_a + \beta_4(\omega_b^2 + \omega_c^2)/12 = 0$. For typical fiber and power parameters, this condition is satisfied if $\omega_s \approx -\omega_2 - (\beta_4/6\beta_3)(\omega_1^2 + \omega_2^2)$. For most pump frequencies, the roots of the polynomial equation are distinct and the (common) range of signal frequencies for which idler generation occurs is of order $|4\gamma P/\beta_3(\omega_1^2 - \omega_2^2)|$. One can produce coincident roots by setting $\omega_1 \approx -\omega_2$, in which case the signal-frequency bandwidth is of order $|4\gamma P/\beta_3(\omega_2 - \omega_1)|^{1/2}$. Notice that the signal-frequency (conversion) bandwidth is limited by β_3, rather than β_4.

In Fig. 6 the signal and idler transmittances are plotted as functions of the signal frequency, for the same fiber and power parameters as Fig. 4. In Fig. 6(*a*) the pump frequencies were

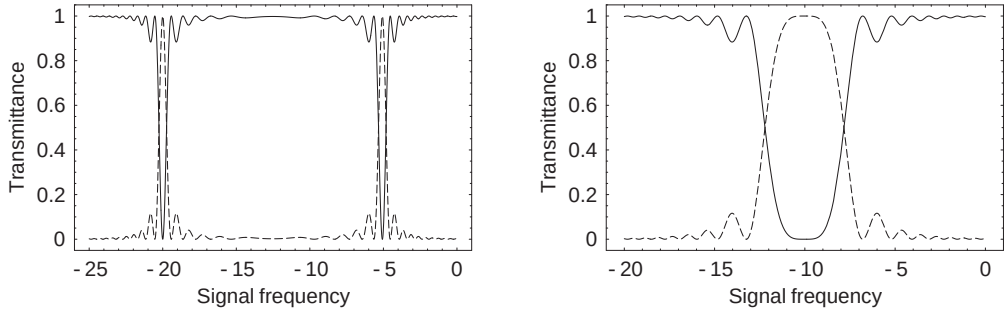

Fig. 6. Signal transmittance (solid curve) and idler transmittance (dashed curve) plotted as functions of the signal frequency ω_s. (*a*) $\omega_1 = -20$ and $\omega_2 = 5$ Tr/s. (*b*) $\omega_1 = -10$ and $\omega_2 = 10$.

chosen to produce distinct signal-conversion bands (distinct roots) for $\omega_s \approx -20$ and $\omega_s \approx -5$ Tr/s. For these values of the signal frequency, the idler frequencies are about 5 and 20, respectively, so the (common) frequency shift is about 25. However, the (common) conversion bandwidth is too narrow to be useful. In Fig. 6(*b*) the pump frequencies were chosen to produce a broader conversion band (coincident roots). As the signal frequency varies from -11 to -9, the idler frequency varies from 9 to 11, so the frequency shift is 20. For the chosen parameters, the conversion bandwidth is still quite narrow. One could obtain better performance by using a fiber with higher nonlinearity or lower third-order dispersion (slope), or pumps with higher powers.

In Fig. 7 the signal and idler transmittances are plotted as functions of the signal frequency, for the same pump frequencies as Fig. 6(*b*). The benefits of higher nonlinearity and higher power are shown in Fig. 7(*a*), whereas the benefits of lower dispersion slope are shown in Fig. 7(*b*). In each case the conversion bandwidth is broad enough to be useful.

6. Translation of polarization-entangled states

The eigenpolarizations associated with BS in a HNF were illustrated in Figs. 2 and 3. If $\delta = 0$ and the pumps are parallel, the BS wavenumber for a parallel signal and idler ($k_\parallel$) is twice the wavenumber for a perpendicular signal and idler ($k_\perp$): Maxima of the perpendicular idler transmittance correspond to minima of the parallel transmittance. Alternatively, if $\delta = 0$ and the pumps are perpendicular, a signal that is parallel to pump 1 (perpendicular to pump 2) produces an idler, whereas a signal that is perpendicular to pump 1 (parallel to pump 2) produces no idler. These dependences of the idler transmittance on the signal polarization makes BS in a HNF unsuitable for the translation of states with two (independent, correlated or entangled)

#8674 - $15.00 USD Received 6 September 2005; revised 26 October 2005; accepted 30 October 2005

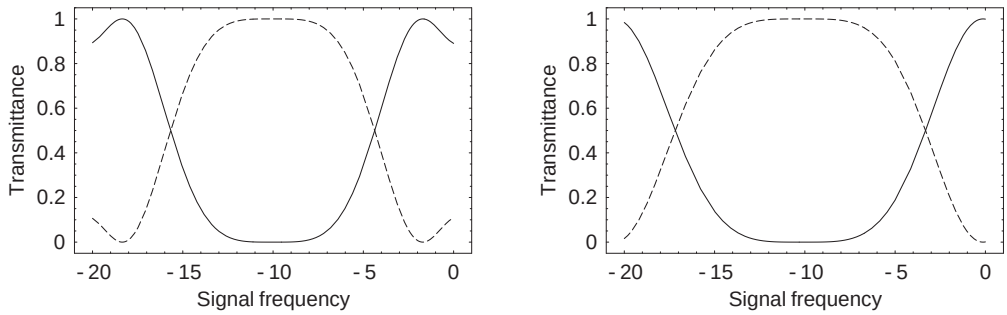

Fig. 7. Signal transmittance (solid curve) and idler transmittance (dashed curve) plotted as functions of the signal frequency ω_s. The pump frequencies $\omega_1 = -10$ and $\omega_2 = 10$ Tr/s. (*a*) $\beta_3 = 0.1$ ps^3/Km, $\gamma = 20$/Km-W and $P = 1.0$ W. (*b*) $\beta_3 = 0.01$, $\gamma = 10$ and $P = 0.3$.

polarization components. The polarization dependence of BS in asymmetric SMFs and MSFs is discussed briefly in the Appendix.

It was demonstrated recently that the idler transmittance associated with BS in a twisted (or spun) SMF, driven by two co-rotating, circularly-polarized pumps, depends only weakly on the signal polarization [15]. This realization of BS is suitable for the translation of polarization-entangled states. BS in a spun fiber is discussed briefly in the Appendix, and its lack of polarization dependence is explained.

7. Noise induced by stimulated Raman scattering

In spontaneous and stimulated Raman scattering (SRS), an incident (pump) light wave with frequency ω_p scatters from a vibration of the medium, with frequency ω, to produce a Stokes light wave with frequency $\omega_p - \omega$ [16]. Typically, the Stokes wave is polarized (predominantly) parallel to the pump [17]. SRS produces noise by amplifying the vacuum fluctuations associated with the Stokes mode and the thermal fluctuations associated with the vibrational mode [18]. It was pointed out recently [19, 20] that SRS increases slightly the noise figures of PAs based on FWM (MI or PC). In a HNF, the SRS bandwidth (range of ω for which amplification occurs) is about 100 Tr/s.

Consider the effects of SRS noise on BS in a HNF. The noise field generated by pump 1 is polarized parallel to pump 1 and (if the anti-Stokes process can be neglected) contains only frequencies lower than ω_1. Hence, it cannot affect the signal (1+) and idler (2+) modes. The noise field generated by pump 2 can affect the 1+ mode directly, but not the 2+ mode. However, the noise component with frequency ω_{1+} is coupled to the component with frequency ω_{2+} by the same BS process that couples the signal and idler. The conditions that maximize the transfer of power from the signal to the idler, namely $\delta = 0$ and $kz = \pi/2$, also maximize the transfer of power from the 1+ component to the 2+ component. Hence, the configuration shown in Fig. 2(*a*) produces an idler that is modified (polluted) by SRS noise. For the configuration shown in Fig. 2(*b*), the noise component with frequency ω_{1+} is polarized parallel to pump 2 and is coupled to the parallel component at frequency ω_{2+}. Because the idler is perpendicular, one could use a polarization-sensitive device to filter out the parallel noise. However, for the optimal case, in which $\delta = 0$, $k_\perp z = \pi/2$ and $|\bar{v}_\perp|^2 = 1$, one does not need to, because $k_\parallel = 2k_\perp$ and $|\bar{v}_\parallel|^2 = 0$: No noise is transferred to the idler. For the configuration shown in Fig. 3(*a*), the noise component with frequency ω_{1+} is perpendicular to pump 1 (parallel to pump 2). As shown in Fig. 3(*b*), this noise component is not coupled to the component with frequency ω_{2+} that is parallel to pump 1 (perpendicular to pump 2): No noise is ever transferred to the idler.

#8674 - $15.00 USD Received 6 September 2005; revised 26 October 2005; accepted 30 October 2005

As stated in Section 6, the signal and idler transmittances associated with BS in a spun fiber do not depend on the polarization of the input signal. Hence, there is always a transfer of power from the noise component with frequency ω_{1+} to the component with frequency ω_{2+}: Polarization-independent translation comes at the price of SRS noise. Although one could use a polarization-dependent device to remove the noise, which co-rotates with the pumps, by doing so one would restore the polarization dependence of BS, which the spun fiber was intended to remove.

The preceding conclusions should be valid in the standard regime, in which the pump powers are moderate, the frequency difference between the pump and Stokes (signal) waves is large, the anti-Stokes source term and the coupling between the Stokes and anti-Stokes waves are weak, and the perpendicular SRS gain is much lower than the parallel gain. Further work is required to model the effects of SRS on BS in the complementary regime, in which nearly polarization-independent SRS was observed recently [21].

8. Summary

In this paper a study was made of optical frequency conversion (translation) by Bragg scattering (BS) in a highly-nonlinear fiber (HNF). In this process, the interaction of two strong pump waves and a weak signal wave produces an idler wave, which is a translated image of the signal. Several combinations of pump and signal polarizations were considered. For the configurations shown in Figs. 2(*a*) and 2(*b*), the idler is generated parallel to the signal. The discussion of Section 7 suggests that in the former configuration the idler is polluted by the noise associated with stimulated Raman scattering (SRS), whereas in the latter it is not. For the configuration shown in Fig. 3(*a*), the idler is generated perpendicular to the signal and is not polluted by noise. If the pump and signal frequencies and polarizations are chosen judiciously, BS in a HNF enables the translation of various individual and frequency-entangled states.

For parameters that are typical of current experiments with HNFs, theory predicts that idlers can be produced with frequencies that differ from the signal frequencies by about 80 Tr/s. If the second-pump and signal frequencies are fixed, the idler frequency can be varied (tuned) by about 30 Tr/s, by varying the first-pump frequency. If both pump frequencies are fixed, signals with frequencies in a range of about 2 Tr/s (standard HNF) or 8 Tr/s (reduced-dispersion-slope HNF) can be converted efficiently. As fiber manufacturing improves, so also will the available signal–idler frequency shift, and the signal tuning and conversion bandwidths.

BS also occurs in birefringent and spun fibers. Because of fiber anisotropy, the properties of BS in a birefringent fiber depend on the signal polarization: BS in such a fiber can be used to translate individual and frequency-entangled states, but cannot be used to translate polarization-entangled states with high fidelity. In contrast, BS in a spun fiber is polarization-independent and can be used to translate individual, frequency-entangled and polarization-entangled states. However, polarization-independent translation comes at the price of SRS noise.

Acknowledgments

CJM thanks J. P. Gordon for his constructive comments on the manuscript. The research of JDH was supported by the NZ Foundation for Research Science and Technology, and the research of SR and MGR was supported by the US National Science Foundation, under contracts ECS-0406379 and ECS-0323141, respectively.

Appendix: Bragg scattering in birefringent and spun fibers

Let **E** denote the electric field vector of a light wave in a fiber and let ω_0 denote a reference frequency, which could be the zero-dispersion frequency (ZDF). Then, associated with ω_0 are the

linear wavenumbers (eigenvalues) $k_\parallel$ and $k_\perp$, and the Jones vectors (eigenvectors) $\mathbf{e}_\parallel$ and $\mathbf{e}_\perp$, which are orthogonal (perpendicular). By measuring frequencies relative to ω_0 and wavenumbers relative to the reference wavenumber $k_0 = [k_\parallel(\omega_0) + k_\perp(\omega_0)]/2$, one can write the field vector as

$$\mathbf{E}(t,z) = \mathbf{A}(t,z)\exp[i(k_0 z - \omega_0 t)], \tag{17}$$

where $\mathbf{A} = \mathbf{e}_\parallel A_\parallel + \mathbf{e}_\perp A_\perp$ is the slowly-varying amplitude vector, and $A_\parallel$ and $A_\perp$ are amplitude components. Interactions between the frequency components of the wave are made possible by the third-order nonlinearity of the medium through which the wave propagates. For an isotropic medium, such as a fiber, the third-order (material) polarization vector

$$\mathbf{P} = \overline{\gamma}[2(\mathbf{A}\cdot\mathbf{A}^*)\mathbf{A} + (\mathbf{A}\cdot\mathbf{A})\mathbf{A}^*]/3, \tag{18}$$

where $\overline{\gamma}$ is the (Kerr) nonlinearity coefficient [22].

For a HNF, $k_\parallel = k_\perp$. As explained in [23, 24], wave propagation in such a fiber is governed approximately by the nonlinear Schrödinger (NS) equations

$$-i\partial_z A_\parallel = \beta(i\partial_t)A_\parallel + \gamma(|A_\parallel|^2 + |A_\perp|^2)A_\parallel, \tag{19}$$

$$-i\partial_z A_\perp = \beta(i\partial_t)A_\perp + \gamma(|A_\parallel|^2 + |A_\perp|^2)A_\perp, \tag{20}$$

where β is the common dispersion function and $\gamma = 8\overline{\gamma}/9$. In the frequency domain $\beta(\omega) = \sum_{n=1}^{\infty} k^{(n)}(\omega_0)\omega^n/n!$ is the Taylor expansion of the common wavenumber about the reference frequency. In the time domain the frequency difference ω is replaced by the time derivative $i\partial_t$. Henceforth, Eqs. (19) and (20) will be referred to as the HNF equations.

By linearizing the HNF equations about an equilibrium that consists of two strong pumps, with frequencies ω_1 and ω_2, one finds that a weak signal, with frequency ω_s, is coupled to a weak idler, with frequency $\omega_i = \omega_s + \omega_2 - \omega_1$. This BS process was studied in [11]. By replacing the classical amplitudes A_s and A_i with the quantal operators a_s and a_i, one obtains Eqs. (3) and (4), upon which Figs. 2 and 3, and the associated text, were based.

Now consider BS in other types of fiber. Birefringent fibers, such as asymmetric SMFs and MSFs, have well-defined polarization axes (x and y). For such fibers $k_x \neq k_y$ and the beat wavenumber $b_0 = [k_x(\omega_0) - k_y(\omega_0)]/2$. By defining $\mathbf{A} = \mathbf{x}X + \mathbf{y}Y$, where $\mathbf{x}$ and $\mathbf{y}$ are linearly-polarized basis vectors, and X and Y are amplitude components, one can rewrite Eq. (18) in the component form

$$P_x = \overline{\gamma}(|X|^2 + 2|Y|^2/3)X + \overline{\gamma}Y^2X^*/3, \tag{21}$$

$$P_y = \overline{\gamma}(2|X|^2/3 + |Y|^2)Y + \overline{\gamma}X^2Y^*/3. \tag{22}$$

In the linear regime, X oscillates in space with wavenumber b_0, whereas Y oscillates with wavenumber $-b_0$. If the beat-length (π/b_0) is much shorter than the interaction length, the third terms in Eqs. (21) and (22) oscillate rapidly relative to the first two, and can be neglected. It follows from these remarks that wave propagation in a highly-birefringent fiber is governed approximately by the NS equations [25]

$$-i\partial_z X = \beta_x(i\partial_t)X + \gamma(|X|^2 + \varepsilon|Y|^2)X, \tag{23}$$

$$-i\partial_z Y = \beta_y(i\partial_t)Y + \gamma(\varepsilon|X|^2 + |Y|^2)Y, \tag{24}$$

where $\gamma = \overline{\gamma}$ and $\varepsilon = 2/3$. Equations (23) and (24) differ from the HNF equations in two ways: A distinction is made between β_x and β_y, and $\varepsilon = 2/3$, not 1. Because these differences are minor, one can deduce results for birefringent fibers from the existing results for HNFs.

The structural similarity of these pairs of NS equations implies that the polarization diagrams of Figs. 2 and 3 also apply to BS in birefringent fibers, with $\parallel$ interpreted as x (or y) and $\perp$

#8674 - $15.00 USD Received 6 September 2005; revised 26 October 2005; accepted 30 October 2005

interpreted as y (or x). For the configuration shown in Fig. 2(a), $\kappa_{\|} = 2\gamma X_1 X_2^*$, whereas for the configuration shown in Fig. 2(b), $\kappa_{\perp} = 2\gamma X_1 X_2^*/3$. For the configuration shown in Fig. 3(a), $\kappa_{\perp} = 2\gamma X_1 Y_2^*/3$, whereas for the configuration shown in Fig. 3(b), $\kappa = 0$. In a birefringent fiber the mismatch $\delta = (\beta_s + \beta_2 - \beta_i - \beta_1) + \gamma(P_1 - P_2)/2$, where each β is β_x or β_y, depending on the polarization of the wave, and each P is a pump power. [This formula does not apply to the configuration shown in Fig. 3(b), but that configuration is of no interest.]

It is customary to assume that the first-order (convection) coefficients in the Taylor expansions of β_x and β_y differ by 2σ, where σ is the group slowness, and the higher-order (dispersion) coefficients are equal. For the configuration show in Fig. 2(a), $\delta_{\|}$ does not depend on σ, because the pumps, signal and idler are all parallel (to the x or y axis) and $\omega_s + \omega_2 - \omega_i - \omega_1 = 0$: BS in a birefringent fiber is no different from BS in a HNF. For the configuration shown in Fig. 2(b), $\delta_{\perp} \propto \sigma(-\omega_s + \omega_2 + \omega_i - \omega_1)$, whereas for the configuration shown in Fig. 3(a), $\delta_{\perp} \propto \sigma(\omega_s - \omega_2 + \omega_i - \omega_1)$: Group-speed difference (GSD) in a birefringent fiber alters (and usually reduces) the tuning and conversion bandwidths of BS. The effects of GSD are stronger for the former configuration than the latter. Notice that $\kappa_{\|} = 3\kappa_{\perp}$: If GSD were absent, $\delta_{\|}$ and $\delta_{\perp}$ could be zero simultaneously, and maxima of the perpendicular transmittances [Fig. 2(b)] would coincide with maxima of the parallel transmittances [Fig. 2(a)]. Although $\delta_{\|}$ and $\delta_{\perp}$ cannot be zero simultaneously, if one could make them small (compared to γP) simultaneously, one could translate polarization-entangled states with reasonable fidelity.

When a fiber is pulled from a rotating preform, a uniform twist (spin) is frozen into the fiber. If the spin period is much shorter than the birefringence beat-length, the fiber behaves (in the linear regime) as an isotropic waveguide capable of transmitting any polarization state unchanged [26]. This statement implies that the wavenumber k, and the associated dispersion function $\beta(\omega)$, are polarization-independent (common). Although the preceding statements are idealizations, they are realistic enough for a preliminary analysis of BS. By defining $\mathbf{A} = \mathbf{r}R + \mathbf{l}L$, where $\mathbf{r}$ and $\mathbf{l}$ are circularly-polarized basis vectors, and R and L are amplitude components, one can rewrite Eq. (18) in the component form

$$P_r = (2\bar{\gamma}/3)(|R|^2 + 2|L|^2)R, \tag{25}$$

$$P_l = (2\bar{\gamma}/3)(2|R|^2 + |L|^2)L. \tag{26}$$

It follows from the preceding remarks that wave propagation in a spun fiber is governed approximately by the NS equations

$$-i\partial_z R = \beta(i\partial_t)R + \gamma(|R|^2 + \varepsilon|L|^2)R, \tag{27}$$

$$-i\partial_z L = \beta(i\partial_t)L + \gamma(\varepsilon|R|^2 + |L|^2)L, \tag{28}$$

where $\gamma = 2\bar{\gamma}/3$ and $\varepsilon = 2$. The only difference between Eqs. (27) and (28), and the HNF equations, is that $\varepsilon = 2$, not 1.

The structural similarity of these pairs of NS equations implies that the polarization diagrams of Figs. 2 and 3 also apply to BS in spun fibers, with $\|$ interpreted as r (or l) and $\perp$ interpreted as l (or r). For the configuration shown in Fig. 2(a), $\kappa_{\|} = 2\gamma R_1 R_2^*$, where the factor of 2 comes from the frequency degeneracy in $|R|^2 R$. For the configuration shown in Fig. 2(b), $\kappa_{\perp} = 2\gamma R_1 R_2^*$, where the factor of 2 comes from the ε in Eq. (28). For the configuration shown in Fig. 3(a), $\kappa_{\perp} = 2\gamma R_1 L_2^*$, whereas for the configuration shown in Fig. 3(b), $\kappa = 0$. In a spun fiber the mismatch $\delta = (\beta_s + \beta_2 - \beta_i - \beta_1) + \gamma(P_1 - P_2)/2$. Notice that $\delta_{\|} = \delta_{\perp}$ and $\kappa_{\|} = \kappa_{\perp}$: BS driven by co-rotating pumps in a spun fiber (Fig. 2) is polarization-invariant. Hence, it can be used to translate polarization-entangled states.

#8674 - $15.00 USD Received 6 September 2005; revised 26 October 2005; accepted 30 October 2005